Giant magnetoresistance in $Fe_{1-x}Co_x/Cr(001)$ trilayers

C. T. Yu, K. Westerholt, K. Theis-Bröhl, V. Leiner, Th. Zeidler, and H. Zabel
Institut für Experimentalphysik/Festkörperphysik, Ruhr-Universität Bochum, D-44780 Bochum, Germany
(Received 12 June 1997)

We have investigated the magnetic and magnetotransport properties of wedge-shaped $Fe_{1-x}Co_x/Cr/Fe_{1-x}Co_x$ trilayers grown by molecular-beam epitaxy on Al_2O_3 $(1\bar{1}02)$ substrates with the Co concentration x ranging from 0 to 0.2. A completely antiferromagnetic (AFM) coupling with zero remanence is obtained in both pure Fe/Cr and alloy $Fe_{1-x}Co_x/Cr$ samples at a Cr thickness of about 10 Å. The giant magnetoresistance (GMR) of the AFM coupled Fe/Cr trilayer is about 5.5% at low temperatures. With increasing Co concentration, the GMR effect, $\Delta\rho/\rho_s$, decreases drastically, having an amplitude of only 0.7% at $x=0.2$. In the pure Fe/Cr trilayer, there is a strong reduction of the GMR effect with increasing temperature. In contrast, the GMR of the samples with alloy magnetic layers is only weakly temperature dependent because of an increase of the net change of the magnetoresistance, $\Delta\rho$, with temperature. The strong decrease of the GMR effect in the alloy trilayers is tentatively ascribed to the possible loss of the band matching of the minority-spin band, which is important in the Fe/Cr superlattice. The temperature dependence of $\Delta\rho$ at finite temperatures can well be interpreted by introducing a positive linear temperature term together with a negative quadratic term, which are attributed to spin-dependent electron-phonon scattering and spin-flip electron-magnon scattering, respectively. [S0163-1829(98)04905-4]

I. INTRODUCTION

Since the discovery of the giant magnetoresistance (GMR) in magnetic multilayers,[1] the origin of the phenomenon has been extensively discussed and it is usually understood in terms of spin-dependent scattering of conduction electrons at the interfaces or within the magnetic layers.[2] The interface scattering is believed to be dominant in CIP-GMR (current in the plane), and CPP-GMR (current perpendicular to the plane) is more sensitive to bulk scattering.[3] Concerning the amplitude of the GMR effect in different multilayers, the mechanisms involved are still subject of discussion.[4] In Fe/Cr superlattices the GMR effect can reach values of more than 200% when the superlattice consists of thin magnetic layers with sharp interfaces.[5] On the contrary, only a very small value of less than 1% of the GMR has been achieved in antiferromagnetically (AFM) coupled Co/Cr superlattices.[6,7]

Theoretical calculations[9,10] considering both spin-dependent scattering[11–13] and spin-polarized electron bands[14,15] in the layered structure revealed that there are two main contributions to the GMR effect. First, the polarized band structure in conjunction with any spin-independent scattering process can produce a large GMR effect, if the Fermi velocities and/or the Fermi surfaces for the minority and majority electrons are different.[10,16] In order to obtain a very large GMR effect it seems that for one of the spin directions the band structure of the ferromagnetic layer and the spacer layer should be similar, i.e., the density of states at Fermi level, the position and dispersion of the electron bands should be nearly identical (band matching effect[17,18]). For the two systems with exceptionally large amplitudes of the GMR effect namely Fe/Cr (Refs. 1,5) and Co/Cu,[19] this situation is realized for the minority-spin band and the majority-spin band, respectively.[18]

The second main contribution to the GMR effect originates from spin asymmetry in the scattering time. Actually there is ample experimental evidence that the spin asymmetry of the interface scattering is the dominant contribution to the GMR effect in magnetic multilayers.[20] Assuming single Cr impurities as scatters in the Fe/Cr interfaces a strong asymmetry in the scattering time for the spin-up and spin-down electron actually has been predicted.[21]

The systematic study of magnetic alloy multilayers, although being rather scarce in the literature, can give information on the mechanism of the GMR effect. Inomato and Saito have shown[22] that the GMR of Co/Cu can be enhanced by alloying Co with a small amount of Fe, but the addition of Ni in $Co_{1-x}Ni_x/Cu$ multilayers was shown to decrease the GMR.[23] The study of $Fe_{1-x}Cr_x/Cr$ multilayers[24] revealed an increase of the GMR at low Cr concentrations. These results have been regarded as an indication that scattering at the random magnetic potential at the interface is the main scattering process for the GMR.[25]

The main goal of the present investigation is a systematic study of the change of the GMR effect in antiferromagnetically coupled $Fe_{1-x}Co_x/Cr/Fe_{1-x}Co_x$ alloy trilayers. To our knowledge, this alloy multilayer has not been reported yet in the literature. In addition to introducing Co point defect scattering, it is expected in a rigid-band picture that the addition of Co will fill the majority band of Fe and change the exchange splitting. This should eventually destroy the matching between the minority-spin band of the Fe and Cr bands, and induce a corresponding change of the GMR effect.

The paper is organized as follows. In Sec. II the sample preparation and the experimental methods are described. In Sec. III we present the main results concerning magnetotransport, magnetic, and structural properties. Discussions about the GMR effect of the $Fe_{1-x}Co_x/Cr/Fe_{1-x}Co_x$ trilayers and its temperature dependence are given in Sec. IV, the conclusion is provided in Sec. V.

II. EXPERIMENTAL METHODS

Using molecular-beam epitaxy (MBE) we have grown $Fe_{1-x}Co_x/Cr/Fe_{1-x}Co_x$ trilayers with a wedge-shaped Cr interlayer on $Al_2O_3(1102)$ substrates with a Cr(001) and a Nb(001) buffer layer. The growth of Nb on sapphire is well established and can be described by the following epitaxial relation:[26]

$$\begin{array}{ccc} Al_2O_3 & & Nb \\ [11\bar{2}0] & \| & [1\bar{1}0] \\ [0001] & \| & [111] \\ [\bar{1}\bar{1}00] & \| & [11\bar{2}]. \end{array}$$

The Cr[110] exactly aligns with Nb[110]. All samples were prepared in a conventional UHV chamber (RIBER, EVA32) designed for metal epitaxy. The base pressure of the system is about 4×10^{-9}Pa and the working pressure is better than 2×10^{-8}Pa. The sapphire substrates have a miscut of less than 1.5°. After chemical etching and rinsing, the substrates were transferred into the introduction chamber and annealed at 500 °C. Afterwards the substrate was annealed again at 1100 °C for 1 h in the preparation chamber. Prior to the growth of the trilayer, a Nb buffer layer of about 100 Å was first grown at 900 °C and then annealed at 950 °C for 30 min in order to achieve a single-crystal growth of Cr and $Fe_{1-x}Co_x$ in the bcc [001] direction. Then a Cr buffer layer of about 100 Å was grown at 450 °C, followed by an annealing step at 750 °C for 30 min. The $Fe_{1-x}Co_x/Cr/Fe_{1-x}Co_x$ trilayer was grown at a substrate temperature of 300 °C. A Cr caplayer of about 50 Å was finally grown to prevent the trilayer from oxidation. Both Fe and Cr were evaporated from effusion cells. The deposition rate was 0.2 Å/s for Fe and 0.16 Å/s for Cr. Co was evaporated by an electron gun with a rate of about 0.02 Å/s, as monitored by an optical rate controller. The $Fe_{1-x}Co_x$ alloy layers were prepared by a simultaneous evaporation of Fe and Co.

The nominal thickness of the magnetic $Fe_{1-x}Co_x$ layers is about 30 Å , the wedge-shaped Cr spacer ranges from about 4.5 to 13 Å with a gradient of 0.16 Å/mm on average over the whole 50 mm long substrates. In the present study we have grown a series of samples with the alloy composition ranging from $x=0$ to $x=0.2$.

The layered structure of the films was characterized by small-angle x-ray reflectivity scans together with quantitative electron microprobe analysis. A medium resolution double-axis diffractometer equipped with a graphite monochromator was used for the x-ray-scattering experiments. For the confinement of the Cu K_α beam size, a horizontal slit of 0.15 mm in width was used together with vertical slits of 0.2 mm. For determination of the Cr wedge thickness, we usually measured the sample at 3 different positions along the wedge. The experimental data were fitted using a modified Parratt formalism incorporating random thickness fluctuations at the interfaces.[27] For confirming the in-plane crystal orientation, grazing incidence x-ray-scattering techniques were used.

For the determination of the alloy composition, we used electron microprobe analysis in a wavelength dispersive mode, which allows the determination of the relative composition of Fe and Co to a much higher resolution than using the energy-dispersive mode.

The interlayer exchange coupling properties of the trilayers were characterized by magnetic hysteresis loops measured via the magneto-optical Kerr effect (MOKE) in a scan mode. For measuring the in-plane component of the magnetization, a longitudinal configuration with an incidence angle of about 45° was chosen. The MOKE signal was determined using a Faraday modulation technique.[28] The rather high modulation amplitude and the use of lock-in techniques provides an angular resolution of better than 10^{-4}degrees.[28] Hysteresis loops were measured in scan steps of 1 mm for magnetic fields along both [100] and [110] of the trilayers.

For the measurements of the magnetoresistance, a conventional four-probe method was employed with the current in the plane (CIP) and the magnetic field applied parallel to the film surface. The specimen studied here were cut from the wedge-shaped sample with a width of about 2 mm (along the wedge direction). For better electrical contacts four gold stripes were sputtered onto the surface of the specimen. Silver glue was used to contact the specimen with gold wires of 0.05 mm in diameter. For measurements at room temperature (about 296 K) and liquid-nitrogen temperature (77 K), the magnetic field was generated by an electromagnet and controlled by calibrated Hall sensor, whereas for measurements at liquid-helium temperatures, a superconducting solenoid was used. All resistivity measurements were made using an ac-lock-in technique, providing a resolution of 10^{-5}. For measurements at liquid nitrogen and room temperature, whole traces of the magnetoresistance loops were taken. In the following, the magnetoresistance ratio is defined relative to the resistivity (or resistance) at saturation fields (ρ_s) as $[\rho(H)-\rho_s]/\rho_s\times100\%$.

III. RESULTS

Figure 1 shows typical small-angle x-ray-reflectivity spectra of the $Fe_{1-x}Co_x/Cr/Fe_{1-x}Co_x$ wedge-shaped trilayers with different Cr thicknesses. The open circles represent the experimental data and the solid lines are fits to the data using a modified Parratt formalism including root-mean-square roughness parameters σ for all interfaces and the surface.[27] The interference fringes are due to the finite thickness of the films. The insets of the figures reproduce the electron-density profile normal to the film surface, which is obtained from the fit and denoted by 2δ with $2\delta=(\lambda^2/\pi)r_0\rho_n(Z+\Delta f)$.[29,27] (Here λ is the wavelength of the radiation, r_0 is the classical electron radius, Z is the atomic form factor, Δf is a dispersion correction, and ρ_n is the density of atoms.)

The thickness and roughness parameters resulting from the fit in Fig. 1 are given in Table I. Starting from the surface the sample consists of a roughly 20 Å thick oxide surface layer, a Cr top layer of about 46 Å, the trilayer comprising two 30 Å thick $Fe_{0.80}Co_{0.20}$ layers with a wedge-shaped Cr spacer in between, a Cr buffer layer of 102 Å and a Nb buffer layer of 62 Å on the average. The Cr wedge has a lateral thickness gradient of about 0.157 Å/mm with 4.3 Å at the thin end and 12.2 Å at the thick end of the sample,

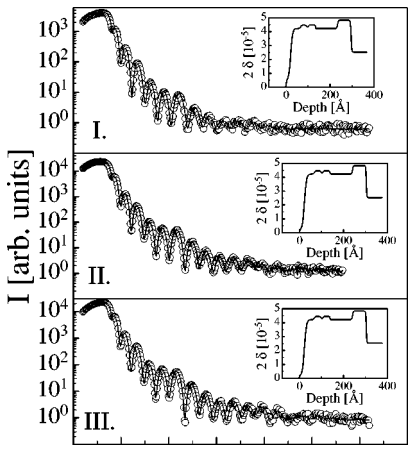

FIG. 1. X-ray reflectivity spectra for an $Fe_{0.8}Co_{0.2}/Cr/Fe_{0.8}Co_{0.2}$ trilayer with a Cr overlayer, a Cr and a Nb buffer layer on sapphire substrates. The scans in I, II, and III were measured from sample positions that are about 5, 25, and 45 mm away from the thin side of a 50 mm long sample. The solid lines are the fits to the data points using a modified Parratt formalism. The insets of the figures show the electron-density profile resulting from the fit.

corresponding to a change of about 1 monolayer of Cr per 9 mm. The interfacial roughness for the individual layer are in the range of 1.2–4.6 Å. Similar measurements of small-angle x-ray reflectivity have been taken for all samples of the present study with the Co concentration $x=0$, 0.03, 0.05, and 0.10. The structural parameters for all samples studied here are summarized in Table II.

For the determination of the interlayer exchange coupling in the $Fe_{1-x}Co_x/Cr/Fe_{1-x}Co_x$ trilayers with varying Cr thicknesses and Co composition, extensive investigations of the magnetic hysteresis loops have been made along both the hard and easy axis, respectively. Figure 2 displays the normalized remanent magnetization as a function of the wedge-shaped Cr thicknesses for the sample $Fe_{0.80}Co_{0.20}/Cr/Fe_{0.80}Co_{0.20}$ as an example. The insets show four representative hysteresis loops measured along the [100] axis. For a Cr thickness less than about 5.2 Å, the hysteresis loop shows only ferromagnetic coupling with a high remanence. With increasing Cr thickness antiferromagnetic coupling starts to become noticeable. For a Cr thickness of about 10 Å, completely antiferromagnetic coupling is realized as indicated by a zero remanence. It should be mentioned that over a large region of the wedge-shaped samples a mixture of bilinear and biquadratic coupling is present.[30] The biquadratic term can be modeled in terms of conventional non-Heisenberg exchange coupling $J_2(\mathbf{S_1}\cdot\mathbf{S_2})^2$. For different Co concentrations the coupling properties with respect to Cr thicknesses are hardly influenced, except for a change of the amplitude of the coupling constant. A complete antiferromagnetic coupling is observed at $d_{Cr}=10$ Å in all samples. It should be noted that the first antiferromagnetic maximum is at 9–10 Å in both Fe/Cr and Co/Cr superlattices. Thus we do not expect a large variation of the position of the first maximum with alloying. The representative hysteresis loops for this position of all $Fe_{1-x}Co_x/Cr/Fe_{1-x}Co_x$ trilayers are sketched on the right panel in Fig. 4. A detailed interpretation of the coupling properties with respect to Cr thickness and Co content will be given elsewhere.[30]

TABLE I. Structure parameters resulting from simulation of the small-angle x-ray reflectivity using a modified Parratt model for sample $Fe_{0.8}Co_{0.2}/Cr/Fe_{0.8}Co_{0.2}$. D and σ denote the thickness of each layer and roughness at each interface or surface, respectively. Position I, II, and III correspond to a distance about 5, 25, and 45 mm away from the thin end of a 50 mm long sample.

	I		II		III	
	D (Å)	σ	D (Å)	σ	D (Å)	σ
Oxide	20.0	1.7	21.6	1.0	21.0	1.0
Cr	45.7	7.4	45.5	7.9	45.6	7.1
$Fe_{0.80}Co_{0.20}$	30.1	4.0	30.7	4.4	30.0	2.9
Cr	5.2	4.6	8.1	4.3	11.2	1.2
$Fe_{0.80}Co_{0.20}$	31.6	2.3	32.1	3.3	31.2	2.6
Cr_{buffer}	101.3	1.0	103.1	2.1	102.8	1.3
Nb_{buffer}	61.4	3.0	62.9	2.8	61.8	1.8
Al_2O_3		2.7		2.4		2.5

TABLE II. Structure parameters of $Fe_{1-x}Co_x/Cr$ trilayers on the AFM coupling position, as derived from small-angle x-ray-reflectivity measurments. D denotes the thickness of individual layer.

	D (Å)				
	$x=0$	$x=0.03$	$x=0.05$	$x=0.10$	$x=0.20$
Oxide	18.7	17.2	16.0	21.0	21.0
Cr	31.5	48.2	29.5	29.7	45.6
$Fe_{1-x}Co_x$	23.6	37	34.3	30.1	30.2
Cr	9.8	10.0	10.5	9.6	9.8
$Fe_{1-x}Co_x$	23.7	37.7	34.8	31.3	31.6
Cr	71.9	121.5	108.2	101.9	102.4
Nb	58.0	92.8	89.6	74.7	62.0

The GMR effect in magnetic trilayers is usually quite small compared to that of multilayers,[31] because trilayers possess less interfaces than multilayers. Therefore, the usual

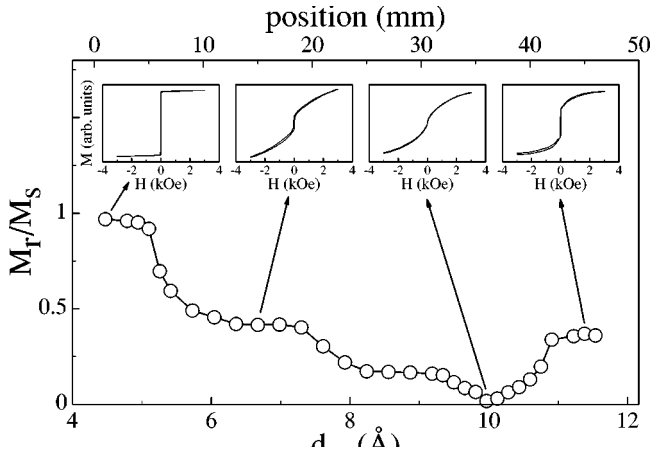

FIG. 2. Normalized remanent magnetization as a function of Cr thicknesses d_{Cr} for the sample $Fe_{0.8}Co_{0.2}/Cr/Fe_{0.8}Co_{0.2}$ obtained from magnetization loops measured by MOKE. The insets show four representative loops for different Cr thickness regimes. A completely antiferromagnetic coupling occurs at about 10 Å. The upper x axis gives the actual position of each measurement along wedge-shaped sample.

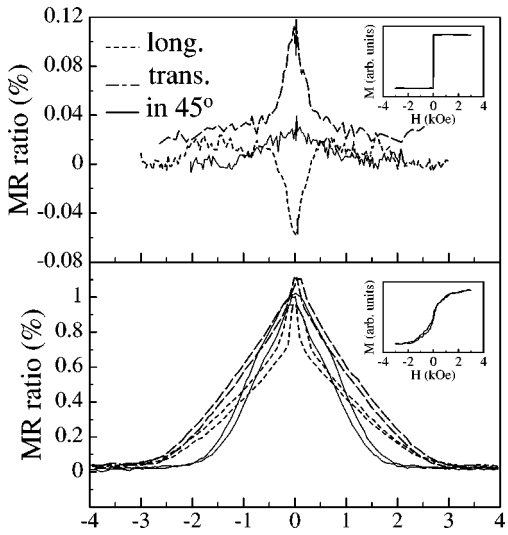

FIG. 3. Magnetoresistance curves measured in different configurations with the current parallel, perpendicular, and in 45° to the magnetic field for samples $Fe_{0.95}Co_{0.05}/Cr$ with different Cr thicknesses: (a) d_{Cr}=5.2 Å with ferromagnetic coupling; (b) d_{Cr}=10.5 Å with antiferromagnetic coupling. The insets of the figures show the magnetic hysteresis loops. For both longitudinal and transverse configurations, the field is applied along [110] axes. For 45°, the field is along [100] axes.

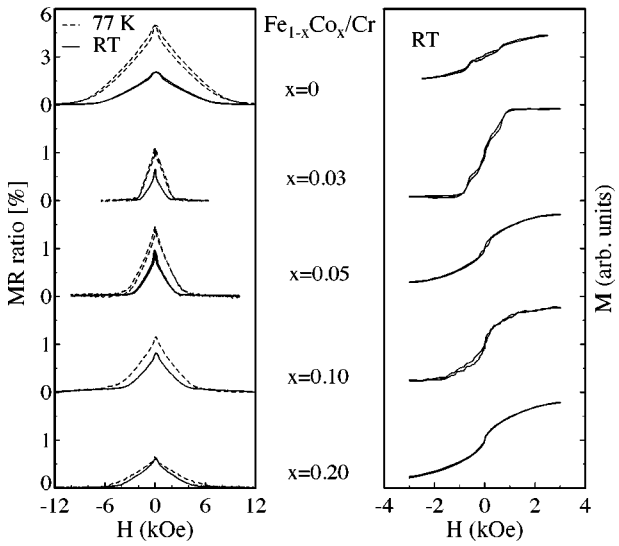

FIG. 4. Magnetoresistance curves for $Fe_{1-x}Co_x/Cr/Fe_{1-x}Co_x$ trilayers with different Co concentrations at room temperature and 77 K, with the external field applied along the hard axis [110] of the films in longitudinal configuration. The related magnetic hysteresis loops obtained from MOKE at room temperature are plotted on the right panel.

anisotropic magnetoresistance (AMR), which depends on the relative orientation between magnetization and sensing current, must be considered, particularly when the Cr thickness is not in the range of complete antialignment of the submagnetizations. For clarifying the AMR effect we have measured the magnetoresistance in different configurations with respect to the angle between the current and the external field.

In Fig. 3, we show the anisotropic magnetoresistance curves for two typical samples of $Fe_{0.95}Co_{0.05}/Cr$ trilayers with ferromagnetic coupling (a) and antiferromagnetic coupling (b), respectively. The insets of the figures show the corresponding hysteresis loops. The magnetoresistance curves are measured in longitudinal configuration, transverse configuration, and in 45° configuration (i.e., the magnetic field was applied at 45° to the current). For the ferromagnetically coupled sample (the upper panel of Fig. 3), only the AMR is observed. For the longitudinal and transverse configuration, the magnetoresistance shows positive or negative slope with the magnetic field, as expected. The AMR effect is ascribed to the spin-orbit interaction and depends upon the angle between the current and the magnetization as $\cos^2\theta$.[32] Therefore, for the measurement in 45° the AMR effect is eliminated approximately as actually seen in the figure. The typical magnetoresistance curves for the antiferromagnetically coupled sample are shown in the lower panel of the same figure. Owing to the AMR effect, the magnetoresistance measured in transverse and longitudinal configuration shows a small reduced and enhanced amplitude, respectively. For all trilayers studied here, the variation of magnetoresistance due to the AMR effect is on the order of 0.1% and thus about an order of magnitude lower than the GMR effect. For the antiferromagnetically coupled samples discussed below, the magnetoresistance is dominated by the GMR effect.

In Fig. 4, we show the MR curves for the AFM coupled position of the $Fe_{1-x}Co_x/Cr/Fe_{1-x}Co_x$ trilayers at room temperature and 77 K. All MR curves shown in this figure were measured in a longitudinal configuration with the magnetic field applied along the [110] direction of the film. From this figure it can be seen that at low fields all MR curves show an apparent jump. This is a typical feature of MR curves with cubic symmetry when the magnetic field is applied along [110] axis.[33] From energy considerations, it corresponds to a magnetic phase transition from an antialigned state allowing only coherent spin rotation to a state with the submagnetizations $\vec{M}_1$ and $\vec{M}_2$ lying in directions symmetrical to the external field direction [110]. At higher fields the MR ratio shows a nearly linear variation with the magnetic field and a well defined saturation field. This feature implies that the influence arising from magnetic disorder at the interface due to roughness is negligible, thus indicating the high quality of the films.

The MR ratio as a function of the Co concentration x is plotted in Fig. 5. For the pure Fe/Cr/Fe trilayer, the MR ratio is about 5 and 2 % at 77 K and room temperature, respec-

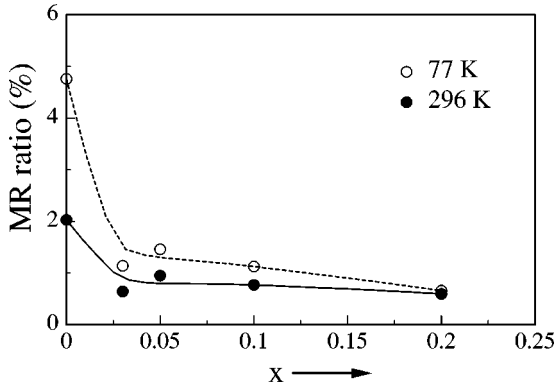

FIG. 5. MR ratio as a function of Co concentration for $Fe_{1-x}Co_x/Cr/Fe_{1-x}Co_x$ trilayers at 77 K and room temperature. The drawn lines are a guide to the eye.

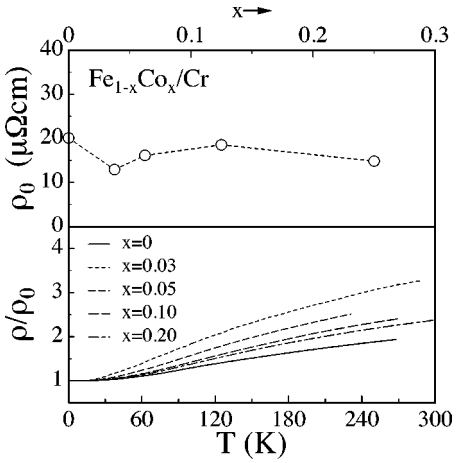

FIG. 6. Upper panel: the extrapolated residual resistivity of the $Fe_{1-x}Co_x/Cr/Fe_{1-x}Co_x$ trilayers as function of x. Lower panel: normalized resistivity of the $Fe_{1-x}Co_x/Cr$ trilayers as function of temperature.

tively. This strong temperature dependence of the GMR effect is consistent with previous reports for Fe/Cr multilayers in the literature.[34] With adding Co the GMR effect decreases drastically and rapidly. Quite surprisingly, even for a small concentration of 3 at. % Co, the GMR effect is strongly suppressed with an MR ratio of only 1.1 and 0.6 % at 77 and 296 K, respectively. With further increase of the Co concentration, the change of the MR ratio is much weaker.

At the first sight, one might assume that the concentration dependence of the GMR effect in Fig. 5 could simply be explained by disorder scattering in the alloy system. However, from Fig. 6, one can see that the residual resistivity for individual samples is irregular with respect to the Co concentration, indicating that the alloy disorder scattering is not the main contribution to the total resistivity of the films. This is easy to understand considering the real structure of the film. As described above, the film consists of eight individual layers with eight interfaces, the magnetic trilayer only has a thickness of about 70 Å compared to a total thickness of about 230 Å for the film. In a resistor array model, the trilayer only contributes about 30% of the conductivity and the main contribution to the residual resistivity ρ_0 comes from the interface scattering. The influence of disorder scattering in the alloy layer arising from Co point defects, which enters into the GMR by adding to the residual resistivity at saturation field ρ_s is not important in these films. The drop of the GMR effect at low Co concentrations must have another origin.

In contrast to the strong reduction of the GMR effect with temperature in Fe/Cr, the alloy $Fe_{1-x}Co_x/Cr/Fe_{1-x}Co_x$ trilayers exhibit a much weaker temperature dependence (see Figs. 4 and 5). For the samples with $x=0.03$, 0.05, and 0.1 the MR ratio decrease slightly between 77 K and room temperature, for the sample with $x=0.2$ the MR ratio at 77 K and room temperature is nearly identical. The temperature dependence of the MR ratio for different Co concentration is displayed in Fig. 7. For pure Fe/Cr the GMR effect is strongly temperature dependent. For the alloy trilayers, however, the MR ratio is only weakly affected by the temperature.

In order to characterize the temperature dependence of the

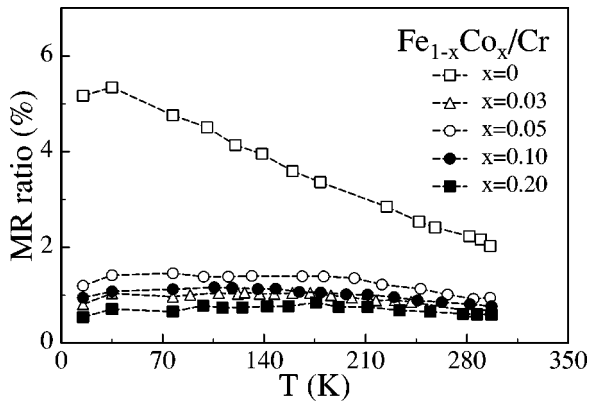

FIG. 7. MR ratio for different $Fe_{1-x}Co_x/Cr$ trilayers as function of temperature. The lines are a guide to the eye.

GMR effect in the $Fe_{1-x}Co_x/Cr/Fe_{1-x}Co_x$ trilayers in more detail, we have plotted the temperature dependence of the net change of the magnetoresistance $\Delta\rho$ in a saturation field and zero field over the temperature regime between 77 K and room temperature (Fig. 8). In this figure, the net change of the magnetoresistance is normalized by the value at 77 K. The temperature dependence of $\Delta\rho$ changes qualitatively when adding Co. For the Fe/Cr trilayer, $\Delta\rho$ decreases monotonously with increasing temperature. For all the alloy $Fe_{1-x}Co_x/Cr/Fe_{1-x}Co_x$ trilayers there is a clear increase of $\Delta\rho$ with increasing temperature up to about 200 K, followed by a slight decrease of $\Delta\rho$ for higher temperatures. Thus, the observed weak temperature dependence of the MR ratio in the trilayers with alloy magnetic layer in Fig. 7 is due to an unusual increase of $\Delta\rho$ with temperature.

IV. DISCUSSION

The main result of the present paper is the strong decrease of the GMR effect in $Fe_{1-x}Co_x/Cr/Fe_{1-x}Co_x$ trilayers, combined with a qualitative change of the temperature dependence of the GMR effect even at Co concentrations as low as 3 at. %. For higher Co concentrations the further change of the GMR is only moderate. We will first discuss the change of the amplitude of the GMR and then come to a discussion of the temperature dependence.

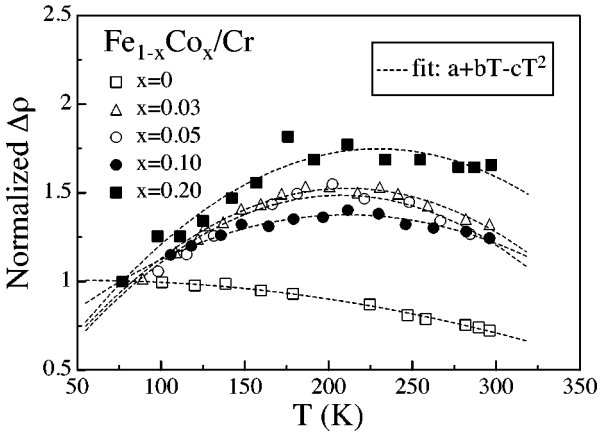

FIG. 8. Normalized net change of magnetoresistance $\Delta\rho$ in a saturation field for different $Fe_{1-x}Co_x/Cr/Fe_{1-x}Co_x$ trilayers. The lines are the fits to the experimental data.

A. The origin of the decrease of the GMR effect

We first stress that the strong decrease of the GMR in $Fe_{1-x}Co_x/Cr$ at low Co-concentration seems to be specific for this alloy system since it has not been observed in other systems like $Fe_{1-x}Cr_x/Cr$, $Co_{1-x}Fe_x/Cu$, and $Co_{1-x}Ni_x/Cu$. First one might assume that this concentration dependence is due to the loss of band matching for the minority-spin band with alloying. As mentioned in the introduction, in the $Fe_{1-x}Co_x$ alloy the majority-spin band is expected to be filled up with increasing x. Here it is helpful to refer to the Slater-Pauling curve as a guide, which shows an increase of the magnetic moment in $Fe_{1-x}Co_x$ with Co concentration up to $x \approx 0.3$.[35] Regarding the density of states for the majority band of Fe,[8] one finds that for filling up the majority band of Fe only about 5% electrons/Fe atoms are required. Thus, the increase of the magnetic moment up to 30 at. % Co is mainly due to a change of the exchange splitting Δ. The change of Δ certainly will change the matching behavior between the Cr bands and the minority band of $Fe_{1-x}Co_x$. If the Cr band lies between the spin-up and spin-down bands of the $Fe_{1-x}Co_x$ alloy, step potential barriers exist for both spin directions. In addition, the band structure itself may undergo modifications on alloying with Co.[36] Both variations can destroy the matching feature and thus diminish the disparity between the potential barriers encountered by the majority and minority spins at the interfaces. This might lead to a reduction of the spin asymmetry in the scattering at the $Fe_{1-x}Co_x/Cr$ interfaces.

However, it seems questionable that only 3 at. % of Co in Fe can cause a definite modification of the band matching behavior in Fe/Cr, resulting in the strong reduction of the GMR effect observed experimentally. The fact that a low concentration of Co in Fe can modify the GMR so strongly suggests that point-defect scattering on Co atoms is very important. For Fe/Cr, a strong asymmetry of scattering by Cr impurities in Fe exists.[21] The addition of Co to Fe causes a partial compensation of the spin-dependent scattering of Cr impurities, because Co impurities in Fe lead to an opposite spin asymmetry of the scattering.[16] This compensation effect will certainly reduce the GMR effect.

B. Temperature dependence of the GMR

As shown in Fig. 6, the temperature dependence of the MR ratio is quite different for the pure Fe/Cr trilayers and for films with alloy magnetic layers. The strong reduction of the GMR effect with increasing temperature is consistent with previous reports in Fe/Cr superlattices,[34,37] and is interpreted by electron-magnon scattering or significant spin fluctuations of local spins,[39] causing spin mixing. In comparison, a less significant temperature dependence of the GMR effect was reported for the Co/Cu superlattice,[38] and attributed to weaker spin fluctuations in Co.[39]

At finite temperature the inelastic temperature-dependent scattering mainly originates from electron-phonon scattering and electron-magnon scattering. Within the two-current model, the electron-magnon scattering leads to a mixing of the two spin channels, thus reducing the magnetoresistance effect. The electron-phonon scattering, however, does not involve spin-flip processes. Therefore, the electron-phonon scattering for the two spin channels can be spin dependent. The electron-phonon scattering rate in Boltzmann theory is given by[40]

$$\left\langle \frac{1}{\tau_{\uparrow(\downarrow)}} \right\rangle = \frac{2\pi}{\hbar} c N_{\uparrow(\downarrow)}(\varepsilon_F) \frac{\langle I^2_{\uparrow(\downarrow)} \rangle}{M \langle \omega^2 \rangle} k_B T. \tag{1}$$

with the spin-dependent density of states $N_{\uparrow(\downarrow)}(\varepsilon_F)$, the mean-square phonon frequency $\langle \omega^2 \rangle$, and the electron-phonon matrix element $\langle I^2_{\uparrow(\downarrow)} \rangle$, which is also spin dependent. If, as for the case of bulk Co,[8] the density of states $N_{\uparrow}(\varepsilon_F)$ and $N_{\downarrow}(\varepsilon_F)$ are very different, the electron-phonon scattering rate for the two spin channels can be different.

The electron-magnon scattering usually plays a more important role at higher temperatures. It was shown[37] that the magnon scattering in antiferromagnetically coupled Fe/Cr superlattices follows a T^2 law well below the Curie temperature.

Approximately, neglecting temperature-dependent electron-electron scattering, the net change of the magnetoresistance at a given temperature can be written as

$$\Delta\rho(T) = \Delta\rho_0 + \Delta\rho_p(T) + \Delta\rho_m(T). \tag{2}$$

Here $\Delta\rho_0$ denotes the primary part of the ground-state GMR effect related to elastic scattering, which is assumed to be temperature independent; $\Delta\rho_p$ is the influence arising from possible spin-dependent phonon scattering; $\Delta\rho_m(T)$ represents the influence coming from electron-magnon scattering which causes spin flip and should yield a negative effect on the GMR.

According to the above assumption, we have fitted $\Delta\rho(T)$ by a second-order polynomial function. The fitting results are plotted in Fig. 8 as broken lines with the fitting parameters listed in Table III. The fit to the experimental data is good with a negative quadratic term and a positive linear term, as expected. This indicates that a common physical effect dominates $\Delta\rho(T)$ in all samples studied here. The positive constant of the phonon term implies that phonon scattering does indeed contribute to the magnetoresistance. The negative constant in the quadratic term for both Fe/Cr and $Fe_{1-x}Co_x/Cr$ samples is consistent with a destructive influence on the GMR effect from electron-magnon scattering. The observation of the anomalous temperature dependence of the magnetoresistance in the alloy $Fe_{1-x}Co_x/Cr$ trilayers is just due to the fact that phonon scattering dominates over the magnon scattering up to temperatures of about 200 K.

TABLE III. Fitting parameters from the simulation of the net change of magnetoresistance as a function of temperature by $\Delta\rho(T) = a + bT - cT^2$ for different $Fe_{1-x}Co_x/Cr/Fe_{1-x}Co_x$ trilayers. For details, see main text.

Samples	*a*	*b*	*c*
MBE812 ($x=0$)	9.93*e*-1	5.11*e*-4	4.86*e*-6
MBE886 ($x=0.03$)	1.05*e*-1	1.34*e*-2	3.17*e*-5
MBE841 ($x=0.05$)	7.24*e*-2	1.36*e*-2	3.29*e*-5
MBE837 ($x=0.10$)	4.64*e*-1	8.64*e*-3	2.04*e*-5
MBE832 ($x=0.20$)	5.69*e*-2	1.47*e*-2	3.21*e*-5

The spin-dependent scattering by phonons can only be observed if the primary GMR effect in the ground state is moderate and the effect from electron-magnon scattering is not too strong. As a result of the spin-dependent phonon scattering, the magnetoresistance $\Delta\rho$ may be enhanced with increasing temperature, as actually observed in all alloy trilayers.

For the Fe/Cr trilayer, the dominant temperature effect of the magnetoresistance $\Delta\rho$ may come from magnons or spin fluctuation at the interface, which causes spin mixing of the two electron channels. The spin-dependent phonon scattering part is less significant because of the comparable density of states (DOS) at the Fermi level for spin-up and spin-down electrons in Fe.[8] With adding Co the majority band will be filled up, and the asymmetry of the DOS at the Fermi level will increase. This, unambiguously, enhances the spin-dependent electron-phonon scattering. On the other hand, adding Co to Fe might stabilize the ferromagnetism at the Fe/Cr interfaces,[41] thus weakening the spin mixing due to spin fluctuations.

V. CONCLUSIONS

In conclusion, we have grown $Fe_{1-x}Co_x/Cr/Fe_{1-x}Co_x$ trilayers on $Al_2O_3(1\bar{1}02)$ substrates in the concentration range of $x=0-0.2$. The structural, magnetic, and transport properties of the trilayers have been investigated by x-ray-reflectivity measurements, MOKE techniques and magnetoresistance measurements. For the pure Fe/Cr trilayer, we observed a GMR effect of about 5.5% at low temperatures. Adding small amounts of Co, the GMR decreases drastically with an amplitude of only 0.7% at $x=0.2$. In contrast to the pure Fe/Cr trilayer, which shows a strong reduction of the GMR effect with increasing temperature, the GMR of the samples with FeCo alloy magnetic layer is weakly temperature dependent because the net change of the magnetoresistance $\Delta\rho$ increases with temperature. The strong decrease of the GMR effect with Co concentration is tentatively interpreted in terms of a band matching effect, which is important for the GMR in Fe/Cr. The unusual temperature dependence of magnetoresistance in $Fe_{1-x}Co_x/Cr$ trilayer with alloy magnetic layers is ascribed to an interplay between spin-dependent electron-phonon scattering and spin-mixing electron-magnon scattering.

ACKNOWLEDGMENTS

This work was supported by the DFG (SFB-166). C. T. Yu acknowledges the Alexander von Humboldt foundation for financial support. We wish to thank A. W. Oswald, J. Ciesielski, and A. Abromeit for technical assistance, and Dr. I. Mertig for helpful discussions.

[1] M. N. Baibich, J. M. Broto, A. Fert, F. Nguyen Van Dau, F. Petroff, P. Etienne, G. Creuzet, A. Friederich, and J. Chazelas, Phys. Rev. Lett. **61**, 2472 (1988).
[2] A. Fert and P. Bruno, in *Ultrathin Magnetic Structure II*, edited by B. Heinrich and J. Bland (Springer, Berlin, 1994).
[3] S. Y. Hsu, A. Barthélémy, P. Holody, R. Loloee, P. A. Schroeder, and A. Fert, Phys. Rev. Lett. **78**, 2652 (1997).
[4] P. M. Levy and Shufeng Zhang, J. Magn. Magn. Mater. **151**, 315 (1995).
[5] R. Schad, C. D. Potter, P. Beliën, G. Verbanck, V. V. Moshchalkov, and Y. Bruynseraede, Appl. Phys. Lett. **64**, 3500 (1994).
[6] W. Vavra, D. Barlett, S. Elagoz, C. Uher, and R. Clarke, Phys. Rev. B **47**, 5500 (1993).
[7] J. J. Picconatto, M. J. Pechan, and E. E. Fullerton, J. Appl. Phys. **81**, 5058 (1997).
[8] A. P. Cracknell, *Metals: Phonon States, Electron States and Fermi Surfaces*, Landolt-Börnstein, New Series III/14c, edited by K.-H. Hellwege and J. L. Olsen (Springer, Berlin, 1984).
[9] W. H. Butler, J. M. Maclaren, and X.-G. Zhang, in *Magnetic Ultrathin Films: Multilayers and Surfaces/Interfaces and Characterization*, edited by B. T. Jonker *et al.*, MRS Symposia Proceedings No. 313 (Materials Research Society, Pittsburgh, 1993), p. 59.
[10] P. Zahn, I. Mertig, M. Richter, and H. Eschrig, Phys. Rev. Lett. **75**, 2996 (1995).
[11] R. E. Camley and J. Barnas, Phys. Rev. Lett. **63**, 664 (1989).
[12] P. M. Levy, S. Zhang, and A. Fert, Phys. Rev. Lett. **65**, 1643 (1990).
[13] R. Q. Hood and L. M. Falicov, Phys. Rev. B **46**, 8287 (1992).
[14] T. Oguchi, J. Magn. Magn. Mater. **126**, 519 (1993).
[15] T. N. Todorov, E. Yu. Tsymbal, and D. G. Pettifor, Phys. Rev. B **54**, R12 685 (1996).
[16] I. Mertig, P. Zahn, M. Richter, H. Eschrig, R. Zeller, and P. H. Dederiches, J. Magn. Magn. Mater. **151**, 363 (1995).
[17] K. B. Hathaway and J. R. Cullen, J. Magn. Magn. Mater. **104-107**, 1840 (1992).
[18] W. H. Butler, X.-G. Zhang, D. M. C. Nicholson, and J. M. MacLaren, J. Magn. Magn. Mater. **151**, 354 (1995).
[19] S. S. P. Parkin, R. Bhadra, and K. P. Roche, Phys. Rev. Lett. **66**, 2152 (1990).
[20] M. A. M. Gijis and G. E. W. Bauer, Adv. Phys. **46**, 285 (1997).
[21] A. Fert and I. A. Campbell, in *Ferromagnetic Materials*, edited by E. P. Wohlfarth (North-Holland, Amsterdam, 1982), Vol. 3.
[22] K. Inomata and Y. Saito, J. Magn. Magn. Mater. **126**, 425 (1993).
[23] H. Kano, Y. Iwasaki, K. Hayashi, and K. Aso, J. Magn. Magn. Mater. **126**, 445 (1993).
[24] B. J. Daniels and B. M. Clemens, Appl. Phys. Lett. **66**, 520 (1995).
[25] J. I. Inoue, H. Itoh, and S. Maekawa, J. Phys. Soc. Jpn. **61**, 1149 (1992).
[26] J. Mayer, C. P. Flynn, and M. Rühle, Ultramicroscopy **33**, 51 (1990).
[27] A. Stierle, A. Abromeit, N. Metoki, and H. Zabel, J. Appl. Phys. **73**, 4808 (1993).
[28] Th. Zeidler, F. Schreiber, H. Zabel, W. Donner, and N. Metoki, Phys. Rev. B **53**, 3256 (1996).
[29] H. Zabel, Appl. Phys. A: Solids Surf. **58**, 159 (1994).
[30] V. Leiner, K. Theis-Bröhl, and H. Zabel (unpublished).
[31] C. P. Potter, R. Schad, P. Beliën, G. Verbanck, V. V. Moshchalkov, and Y. Bruynseraede, M. Schäfer, R. Schäfer, and P. Grünberg, Phys. Rev. B **49**, 16 055 (1994).

[32] D. P. Thompson, IEEE Trans. Magn. **MAG-11**, 1039 (1975).
[33] W. Folkerts, J. Magn. Magn. Mater. **94**, 302 (1991).
[34] F. Petroff, A. Barthelemy, A. Harmzic, A. Fert, P. Etienne, S. Lequnien, and G. Creuzet, J. Magn. Magn. Mater. **93**, 95 (1991).
[35] T. R. McGuire and D. I. Bardos, J. Appl. Phys. **40**, 1371 (1969).
[36] J. Kanamori, H. Akai, N. Hamada, and H. Miwa, Physica B & C **91**, 153 (1977).
[37] J. E. Mattson, M. E. Brubaker, C. H. Sowers, M. Conover, Z. Qiu, and S. D. Bader, Phys. Rev. B **44**, 9378 (1991).
[38] M. A. M. Gijs, S. K. J. Lenczowski, R. J. M. van de Veerdonk, J. B. Giesbers, M. T. Johnson, and J. B. F. aan de Stegge, Phys. Rev. B **50**, 16 733 (1994).
[39] H. Hasegawa, Phys. Rev. B **47**, 15 073 (1993); H. Hasegawa, J. Appl. Phys. **79**, 6376 (1996).
[40] J. M. Ziman, *Electrons and Phonons* (Oxford University Press, Oxford, 1979).
[41] R. Coehoorn, J. Magn. Magn. Mater. **151**, 341 (1995).